# Framework for Unknown Airport Detection in Broad Areas Supported by Deep Learning and Geographic Analysis

Ning Li, Liang Cheng, Lingyong Huang, Chen Ji, Min Jing, Zhixin Duan, Jingjing Li, and Manchun Li

***Abstract*—Airports serve as important economic and military facilities, and thus, their spatial distribution can strongly impact people's lives and social economy. However, existing airport databases have incomplete information and low accuracy rates owing to the high cost associated with updates and lack of timely information. Due to the complexity of broad-area scenes, the accuracy of airport detection using only image recognition is extremely low. This article proposes a framework for detecting unknown airport distributions in a broad research area based on deep learning and geographic analysis. First, we extracted correct points from an existing airport database, and a positive and negative scene classification model based on Google image data was trained to scan and extract candidate airport regions. Next, the airport confidence was evaluated to extract the positions of airports in the candidate area. Simultaneously, geographical data such as road networks and water systems were used to comprehensively analyze the detection results. For the 21 9040.5 km$^2$ (Jiangsu, Shanghai, Zhejiang) study area, the recall rate of known airports of this framework was 96.4%, and the airport integrity rate was 97.2%. The speed was approximately 20 times faster than that of traditional visual searches. Through systematic comparison, eight airports were newly discovered; however, one established database airport was missing. The results demonstrate that the proposed framework can validly detect unknown airports with high accuracy in a broad area and concurrently, expand the applications of deep learning, remote sensing, and geography.**

***Index Terms*—Broad area, candidate area extraction, deep learning, geographic analysis, remote sensing, unknown airport detection.**

Manuscript received December 1, 2020; revised March 6, 2021; accepted June 7, 2021. Date of publication June 14, 2021; date of current version July 1, 2021. This work was supported in part by the National Key Research and Development Plan under Grant 2017YFB0504205 and in part by the National Science Foundation of China under Grant 41622109. *(Corresponding author: Liang Cheng.)*

Ning Li, Liang Cheng, Chen Ji, Min Jing, Zhixin Duan, and Manchun Li are with the Jiangsu Provincial Key Laboratory of Geographic Information Science and Technology, Key Laboratory for Land Satellite Remote Sensing Applications of Ministry of Natural Resources, School of Geography and Ocean Science, Nanjing University, Nanjing 210023, China, with the Collaborative Innovation Center of South China Sea Studies, Nanjing 210023, China, with the Jiangsu Center for Collaborative Innovation in Geographical Information Resource Development and Application, Nanjing 210023, China, and also with the Jiangsu Center for Collaborative Innovation in Novel Software Technology and Industrialization, Nanjing 210023, China (e-mail: 1067103674@qq.com; lcheng@nju.edu.cn; jichen@smail.nju.edu.cn; jmhwxyshpy@163.com; dzx224@163.com; limanchun@nju.edu.cn).

Lingyong Huang and Jingjing Li are with the China Centre for Resources Satellite Data and Application, Beijing 100094, China (e-mail: hlylj87@126.com; 595926530@qq.com).

Digital Object Identifier 10.1109/JSTARS.2021.3088911

## I. Introduction

As AN important piece of military and civil infrastructure, airports play a vital role in aircraft landing, transportation, and energy supply [1]. In recent years, airport detection has gained increased attention and has become a topic of interest in computer vision and remote sensing research [2]. A fast and automatic airport detection method at regular intervals can be highly useful because existing airport databases are incomplete and have a high update cost [3]. Using high-resolution remote sensing images to identify airport targets is of substantial importance for obtaining airport information that is highly current and has a strong integrity. Several previous studies have been based on single images [1], [2], [4]–[7], including those on the detection of some small objects [8], [9], but these methods are not suitable for broad area searches. The broad area of research that airport recognition scholars generally focus on is still based on single images or a slightly larger range of spliced images, which is different from the concept of large regional areas. Some scholars have also used impervious surfaces to extract candidate areas combined with aircraft identification to perform broad area airport identification [3], but this is not applicable to airports without aircraft. Because of the complex background and the considerable work inherent in identifying broad areas, it is a challenging task to discover complete airports in a broad area.

Many scholars have performed several constructive works on broad area target detection [3], [10]–[13]. Zeng *et al.* [3] used fine resolution observation and monitoring of global land cover 10 [14] (FROM-GLC10) data to extract airport candidate areas, and a Faster-RCNN aircraft detection framework [15] was utilized to determine the airport location. In addition to using remote sensing products for candidate areas, deep convolutional neural networks (DCNNs) provide strong support for preliminary candidate area screening. Yuan *et al.* [10] introduced an approach based on deep convolutional networks that effectively delineated solar panels in aerial scenes. Marcum *et al.* [11] combined RESNET 101 DCNN [16] with spatial clustering to efficiently search for missile positions in the Southeastern China Research Area; this method was 81 times more efficient than traditional visual search. Yu *et al.* [12] divided target solar panels to be extracted into positive and negative samples and adopted the deep learning scene classification method for pre-extraction. Scott *et al.* [13] used the trained DCNNs [16], [17] model to classify objects of interest in a broad area and obtained accurate results. All the above methods have a positive effect on the extraction of candidate regions for target detection in broad areas.

After obtaining a candidate area, the airport location becomes the basis and key to the final production of an airport database. From the perspective of target detection, general airport facilities include aircraft, runways, terminal buildings, and aprons. Accordingly, previous studies have used aircraft [3], [18]–[26] to identify airports; however, these methods do not consider the absence of aircraft in an airport, resulting in airport detection loss. There are also several studies that regarded an entire airport or runway as a representative to locate other airports [2], [4]–[6], [23], [27]–[35]. From the perspective of extracting airport feature levels, airport detection can be divided into two categories. One is traditional methods [4]–[7], [18], [19], [22]–[24], [27], [28], [30]–[32], [36], [37], which extract the low-level features (visual saliency, line segment features, spectral features, textural features, geometrical characteristics, multiple features, etc.) of the airport in the image. The other is deep learning methods [2], [3], [20], [21], [23], [25], [26], [29], [33], [34], [38], which extract high-level features (deep convolution features). Although some traditional methods [5], [6], [30] have demonstrated an accurate performance, they are excessively time-consuming and cannot support broad area identification work. Regarding deep learning methods, the detection times of YOLO [39]–[41] and SSD [42] based on deep learning target detection are lower than those of Fast R-CNN [43] and Faster R-CNN [44], which are more suitable for broad area detections.

Extracting airport locations from a large area will inevitably lead to many false extractions. Zeng *et al*. [3] first restricted the distribution of airports by their impervious surface characteristics using FROM-GLC10 [14]. In addition to the constraints of impervious surface characteristics, airport construction should consider the accessibility analysis of roads [45], and different roads have unique attributes owing to their varying functions. For example, the properties of airport roads and general roads in Open Street Map [46] (OSM) data differ, and general airport roads or roads near the airport are classified as service properties. Concurrently, Zeng *et al*. [3] also states that impervious surface features constitute one of the important feature types of the airport, so the distributions of the airports and water systems are mutually exclusive. Overall, there is a spatial distribution constraint relationship between the location of the airport and certain geographic data.

In order to improve the accuracy of the existing methods and the detection ability of features in broad areas, a framework combining deep learning and geographic analysis is proposed in this article: candidate area extraction with scene classification in a broad area, airport positioning with confidence evaluation on a small scale, and comprehensive judgment with geographic analysis. The main contributions of this study are summarized as follows.

1) For broad areas, we propose a framework for rapidly mining unknown airports to form an airport database with complete information and high accuracy.
2) Methods such as deep learning (scene classification and object detection), feature fusion, and geographic analysis are integrated to extract airports, which expands the applications of deep learning, remote sensing, and geography.

TABLE I
DATA MATERIALS OF THIS PAPER

| Type | Source | Count |
|---|---|---|
| airports locations | OurAirports (OA, https://www.ourairports.com) | 35 (initial), 28 (locations with runway) |
| tiles | Google Earth (level 17) | 4005440 |
| roads | Open Street Map (OSM, http://download.geofabrik.de/) | 441445 |
| water | Open Street Map (OSM, http://download.geofabrik.de/) | 21597 (polyline), 57120 (polygon) |
| administrative boundary | GADM (https://gadm.org/index.html) | - |

The remainder of this article is organized as follows: Section II briefly introduces the research area and materials and describes the method and content of the airport detection framework in detail. Results and discussion are given in Sections III and IV, respectively. Finally, Section V concludes the article.

## II. Materials and Framework

### A. Materials

Relevant experiments are conducted in Jiangsu, Shanghai, and Zhejiang Provinces in China (see Fig. 1). The three regions have areas of 107 200, 6340.5, and 105 500 km$^2$, respectively, and the total area of the studied regions is 219 040.5 km$^2$. As one of the most important developed economic zones in China, Jiangsu, Shanghai, and Zhejiang have a higher density of airport construction compared to other areas, and the framework and models established are more robust. As summarized in Table I, the airport data comprises public datasets as samples and verification references and can be found in the public OurAirports (OA) airport dataset.[1] In addition, all the airport locations obtained from the OA database in the study area are visually verified. Initially, there are 35 OA locations in our study area, which includes large airports, medium airports, small airports, heliports, and closed airports. After verifying the correctness of these points using Google imagery, finally, 28 points with evident runway characteristics as the correct data are selected. For remote sensing image data, we download 17 levels of Google image data in the study area, with 4 million tiles total and a total data volume of 51G. The OSM data are extracted from OSM;[2] roads, and water (polyline, polygon) data are mainly used. GADM[3] provides the administrative boundary data of the study area.

### B. Framework

This article proposes a calculation framework for unknown airport target detection in broad area scenarios that combines

[1][Online]. Available: https://www.ourairports.com
[2][Online]. Available: http://download.geofabrik.de/
[3][Online]. Available:https://gadm.org/index.html

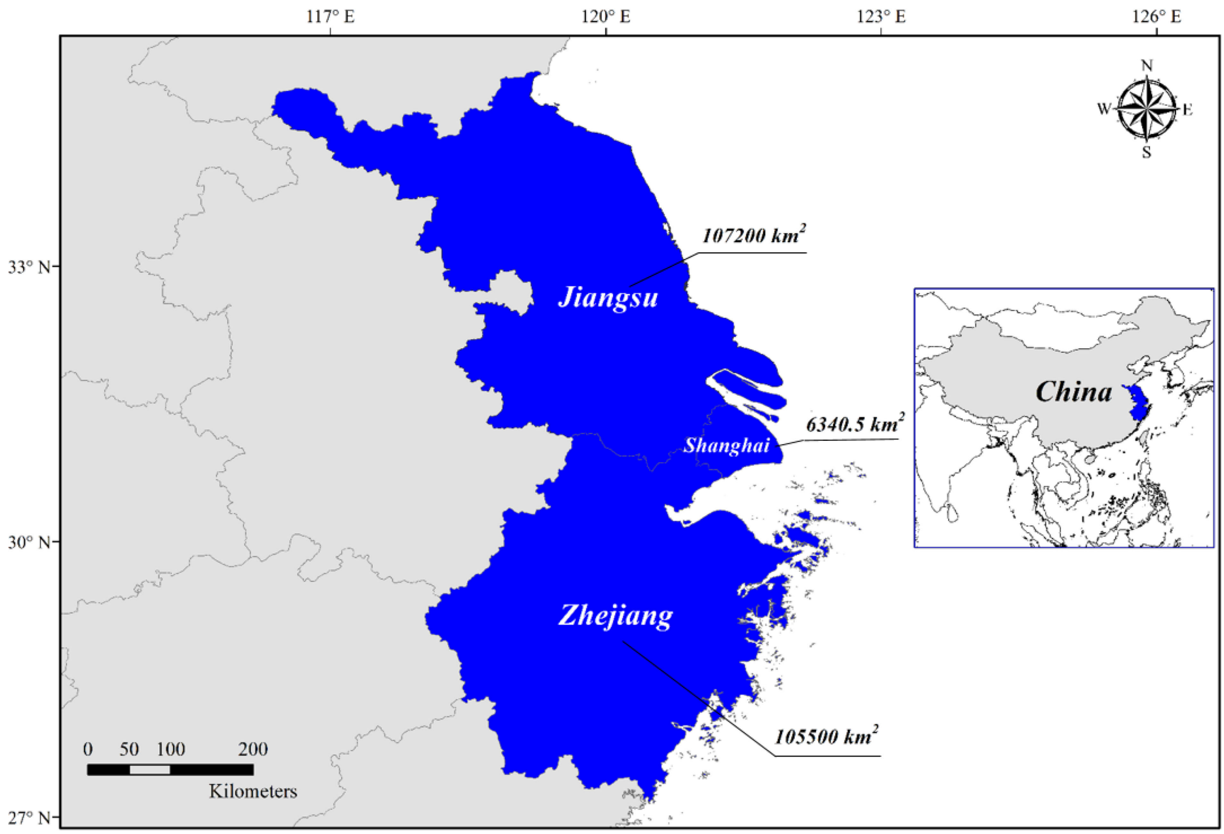


Fig. 1. Experimental areas in eastern China, including Jiangsu, Shanghai, and Zhejiang.

deep learning and geographical analysis (see Fig. 2). The first is the extraction of candidate areas for the detection of airport targets, which is used as a target area screening task and can greatly reduce the workload of identification tasks. In this step, we apply the scene classification model and use the airport pattern features with impervious surfaces and the non-airport pattern features in the research area to obtain the airport-oriented two-class classification model. Then, a "push-broom" search on Google tiles of large area scenes is performed. After the scene is classified and analyzed, an airport target candidate area is obtained. The next part is the detection of target airport features. The airport runways are taken as the main feature and the aircraft as the auxiliary features to evaluate the airport confidence supported by deep learning models while performing a comprehensive judgment of the geographic information about the candidate area. The geographic analysis constrains the direction results by extracting the main direction of the line segment and applying OSM, coastline spatial distribution, geographic threshold, etc., to calculate the geographic limit of the main feature. Finally, the results are systematically verified to extract the unknown airports in the broad research area.

*1) Candidate Area Extraction:* To obtain an effective sample library, the public OA information is utilized as basic data, which is visually judged for correctness in the images. The validated data are used as the valid airport point data in the study area, and part of it is extracted for the scene classification sample base. In the visual extraction process, the runway is regarded as the main feature of the airport. By judging whether the area contains an airport runway and retaining the airport with runway salient features, large airports, medium airports, small airports, and closed airports are likely to be included in the verification data. Moreover, the road network and water system in the OSM data are calculated to generate geographical analysis, and this process will be described in detail in the following chapters.

The extraction of candidate regions in a large space area is one of our key goals. Airport tiles with a specific resolution are distinguished from other features in the image. Our goal is to achieve specific target detection in the research area. Therefore, the two-classification method (see Fig. 3) is used to classify different features in the research area. In the method proposed in this article, the scene classification model is applied to classify and predict Google image data. Furthermore, to reduce the area of interest for target detection in a large area, factors such as spatial scale are utilized to analyze and provide high-confidence candidate areas for subsequent geoscience analysis and airport detection. We utilize the binary classification method by selecting the airport data with the correct points extracted in 2.1, download the fixed range ($0.04° \times 0.04°$).

Google 17-level (ground resolution of approximately 1 m) tile images and divide the Google airport tiles into airport (airport) and non-airport categories (non-airport), as shown in Fig. 3. The airport category is considered as a positive sample for scene classification, which mainly includes runway tile scenes and other scenes with evident airport impervious surface features.

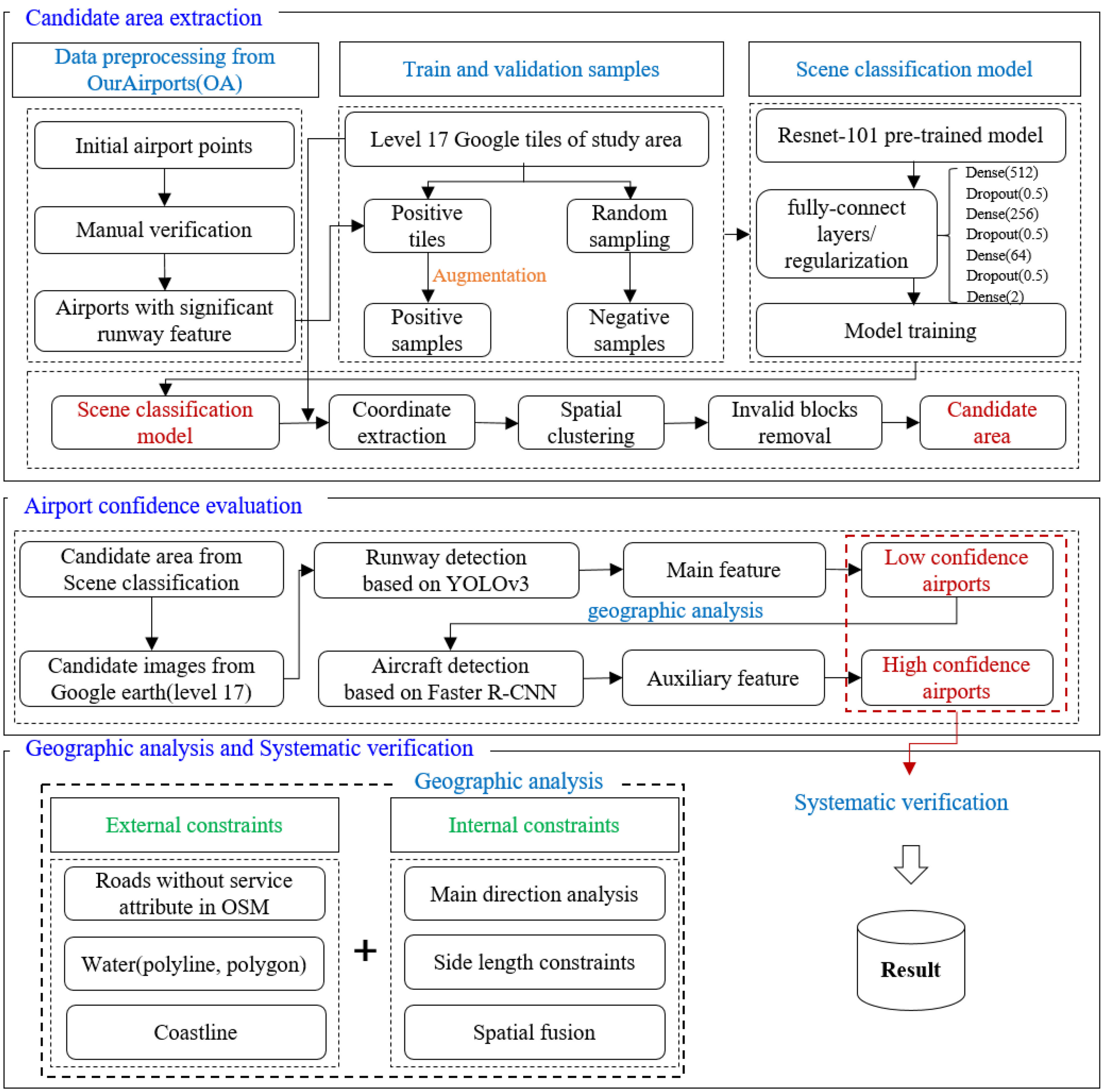


Fig. 2. Framework for airport detection in a broad area.

For nonairport categories, considering that negative samples are required to contain the global characteristics of the research area, the entire research area is a negative sample candidate area. A total of 4.4 percent of the data is selected as negative sample data (no intersection with the positive sample). Concurrently, to ensure that the negative and positive samples meet the balance of the positive and negative sample data volume, we perform a dilution of the selected negative sample, and data enhancement and data balancing work are applied to the positive sample.

In order to obtain an effective scene classification model, the RESNET DCNN pretrained model based on the ImageNet large-scale sample dataset is applied as the basic classification network. The RESNET network structure was proposed in 2015 and won first place in the ImageNet classification task competition. Through transforming the output classification layer of the model, the goal of classification and detection is achieved. The purpose of using the pretraining model is to make full use of the weight of the pretraining network, improve classification accuracy, and increase the speed of model training.

Specifically, the two-classification framework is based on the ResNet101 DCNN [16] pretraining model of the ImageNet large-scale sample dataset as the basic classification network, and it accesses the following four fully connected classification layers (with the number of output categories in parentheses): dense (512), dense (256), dense (64), and dense (2). In addition, the dropout regularization method is adopted to constrain

TABLE II
DATA AUGMENTATION FOR SCENE CLASSIFICATION

| Type | Initial | Method | Augmentation | Train | Validation |
|---|---|---|---|---|---|
| AIRPORTS | 1234 | copying noising flipping rotating | 95018 | 85547 | 9471 |
| NON-AIRPORTS | 175247 | - | 175247 | 157723 | 17524 |

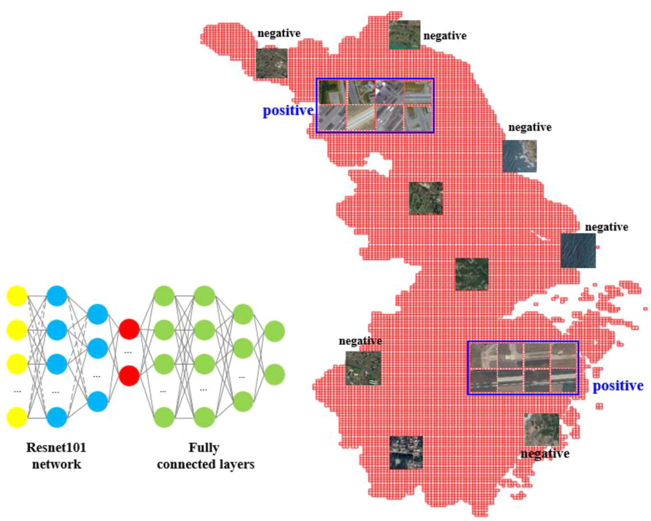


(a) (b)

Fig. 3. Two-classification methods and samples. (a) Schematic diagram of the two-classification model networks. The front end is the Resnet101 basic network, and the back end is connected to the fully connected classification layers. (b) Some examples of positive samples and the grid segmentation of the study area to extract negative samples.

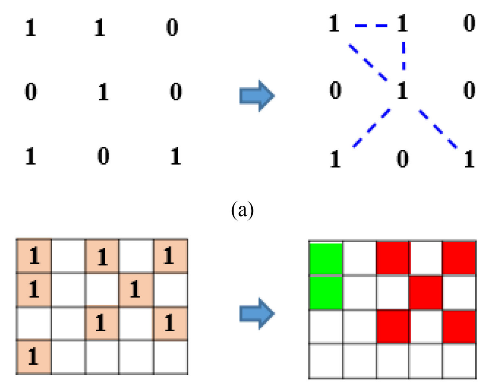

(a)

(b)

Fig. 4. Eight-direction connectivity analysis. (a) Eight-direction connectivity. (b) Spatial clustering and filtering after eight-direction connectivity analysis.

the parameters between every two classification layers. After training, a two-class classification model for broad area scenes is obtained and a "push-broom" search on approximately 4 million tiles is performed in the study area. If the classification probability of a grid tile is greater than 0.5, it is considered an airport scene; otherwise, it belongs to another nonairport scene.

For getting valid training data, the 28 verified airports are selected in the study area. After screening, the tiles with impervious surface characteristics of airports are taken as positive samples, and a total of 1234 positive samples are found. To consider the overall characteristics of the negative samples in the study area, approximately 175 247 tiles with negative sample tile data are randomly selected from the entire study area; they are then used to characterize the scene characteristics in the study area that do not correspond to those of airports. Considering the balance of data volume between sample categories, copying, noising, flipping, rotating, etc., are used to enhance the data of the positive samples. The positive sample size is expanded from 1234 to 95 018, and the data volume of negative samples remains unchanged. Concurrently, approximately 10% of both positive and negative samples are extracted as the dataset for verification. The specific situation is summarized in Table II.

The tile classification probability is obtained by classifying the tile scenes of a broad area, and the geographic coordinates of each tile are further calculated to obtain a collection of points of interest in the airport area. Considering that the spatial resolution of the 17-level Google image is approximately 1 m, the Google image tile pixels are 256∗256, and the shortest airport runway length approximately generally about 500–1000 m, there is, thus, an adjacency relationship between airport points; more specifically, under normal circumstances, the airport points of normal classification should be nonoutlier. According to the airport construction specifications, the direction range of the airport runway is [0360]. Using eight-direction connectivity analysis (see Fig. 4), the interest areas with spatial proximity relationships are connected to achieve geographic spatial clustering of interest points in the airport area.

In the process of spatial clustering, it is also found that for tile images with a resolution of approximately 1 m and 256∗256 pixels, the width of an isolated classification point is approximately 256 m, and the shortest runway length is generally between 500–1000 m; therefore, the number of correctly classified points of interest obtained should be greater than or equal to 2 with the airport runway classified by the grid scene. Next, patches with more than two spatial connection points after cluster analysis are selected to perform the preliminary extraction of airport candidate areas.

*2) Airport Confidence Evaluation:* The candidate area of the airport target is obtained after performing the calculation described above. As they are the most evident characteristics of an airport, the runway and aircraft with considerable prominence play an important role in airport detection [3], [47]. Airports with runways may not have aircraft, but airports that have aircraft but no runways are less common; therefore, the latter is regarded to be of little significance, and runways are considered the main feature and the aircraft are considered the auxiliary feature to increase the airport confidence. As one of the representative frameworks for target detection, YOLO [39]–[41] has a fast detection speed and low background false detection rate. In order to realize runway detection, YOLO-v3 [41] along with a darknet-53 neural network is applied to construct the basic framework, which is achieved in Ji *et al*. [47]. And then the runway detection results are constrained by geographic analysis, which will be detailed in the next section. After the analysis, the aircraft detection model based on Faster R-CNN [3] is used for airport detection as the detection of auxiliary features such as aircraft improves airport confidence. We believe that the detected airport has the highest probability of actually being an airport if it has the above two features, followed by the airport in which only the runway is detected, and the area in which only aircraft were detected are not be counted. Obviously, airports with high confidence have a greater probability of being used and, therefore, are more important.

*3) Comprehensive Geographic Analysis:* Ensuring the correct detection of the main feature is crucial to the framework. The results of airport detection often contain misclassified features such as roads, water systems, canals, and farmland. These incorrect detection results will have a substantially negative effect on the final detection accuracy, so the rationality of these results is the focus. Considering that runways and certain ground objects constitute mutually exclusive elements, there are constraints on the relationships between them and their spatial distribution. For example, the runway should not cross roads, rivers, coastlines, etc. Based on these constraints on the spatial relationships between the runways and roads, water systems, and coastlines, this rule is adopted to eliminated misclassified features among the detected airports. This specific method of relying on limitations of external features is referred to as external constraints. Also, the line segments of the image corresponding to the runway detection boxes are extracted and their main direction angles are counted. The angle difference between the main direction and the detected runway direction is calculated later, if the difference between the two is excessively large, the detection result is regarded as a detection error and ruled out. Next, in the detection results, the runway detection box of unreasonable length also needs to be removed. Finally, each airport has a certain range of influence, more specifically, the distance between two airports should not be excessively small. Otherwise, they will be regarded as the same airport. Based on the above criteria, the results of airport detection in the study area are extracted. These methods of using limitations based on the airport itself are called internal constraints.

In the runway detection results, the diagonal line in the detection frame is regarded as the main runway, but the main direction information of some images did not match the runway direction in the detection. Based on this phenomenon, the LSD [48] straight line detection algorithm in the Google images (level 17, and the ground resolution is about 1.2 m) is adopted to detect straight line segments after which the main direction of the detected line segments is obtained. To ensure correct detection, the angle between the main direction and the diagonal direction in the detection frame should not be excessively large. We extract the main directions of 28 known airports and calculate the difference between the main directions and the runway directions. It was found that the maximum difference between them is 8.5 degrees. Considering the robustness, a coefficient of 2.5 is used to amplify the allowable difference between the main direction and the airport runway direction, so the difference boundary becomes 21.25 degrees. The recommended difference threshold in this article is 20 degrees. Therefore, a box is eliminated if the angle is greater than the threshold, otherwise, it is retained.

Similar to the main direction constraint relationship, when using the spatial distribution relationship constraint, the diagonal line in the detection frame is also used as the detection result. The roads and water in the OSM data are computed to constrain the detection results. Notably, a part of the airport road data is reflected in the OSM road network data as the service attribute. Therefore, when calculating the spatial relationship, roads that do not contain the service attribute are utilized. Considering that most of the study area is close to the sea and the coastline is also easily misidentified; therefore, the coastline data from administrative boundaries are extracted and combined with OSM data to provide a joint constraint.

In the runway detection results, there are also some unreasonable runway lengths, so some side length constraint rules are applied to eliminate them. Among the known runway detection results of 28 airports, the shortest long edge is approximately 1543 m, and the shortest short edge is approximately 150 m. Considering the existence of some small airports, the coefficient 2.5 is used to scale the long side, so the minimum threshold for the long side is approximately 620 m, and the minimum threshold for the short side is approximately 150 m.

For spatial fusion, in contrast to the aforementioned geographical constraints for individuals, some of the identified runways are excessively close, so the runways in this situation are spatially fused; more specifically, runways with a distance less than a certain threshold are considered as belonging to the same airport. We set this threshold at 4 km.

## III. Results

### A. Candidate Area Extraction Results

We extracted 17 930 points from 4 million tiles in the study area. After obtaining the classification information of the airport scene in the study area, the geographic information of the airport scene points in the study area was calculated. Considering Google image resolution and airport runway length constraints, an eight-direction connectivity analysis on the airport interest points in the study area was performed to group adjacent interest points to achieve spatial clustering of interest points. Finally,

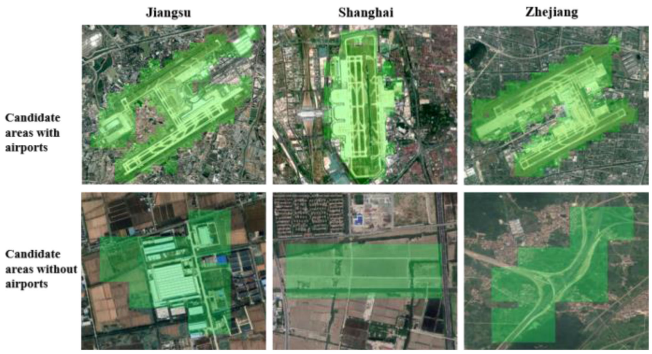


Fig. 5. Example results of scene classification and post-processing in Jiangsu, Shanghai, and Zhejiang.

Fig. 6. Detection results of known airports.

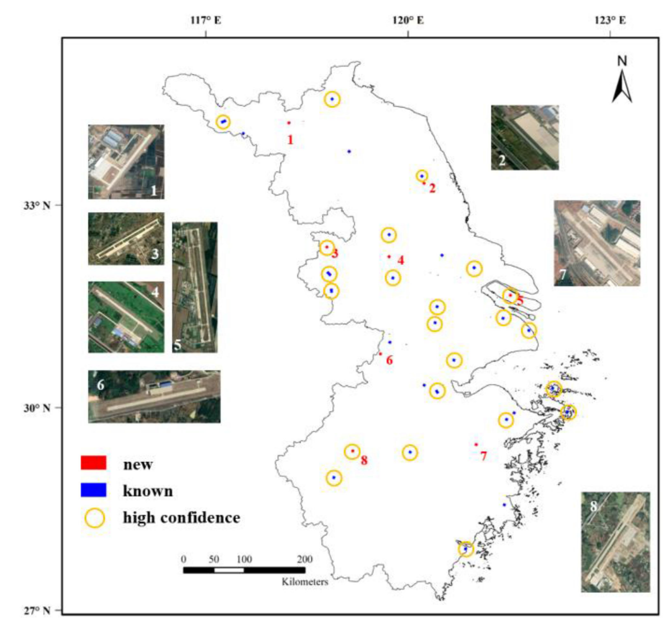


Fig. 7. Framework results and newly discovered airport images.

we aggregated 17 930 instances of point information into 9166 spatial groups.

For the spatial group obtained by spatial clustering, if there were no adjacent points of interest around a certain point of interest, an isolated point was formed. For such situations, the spatial range could not cover a complete airport range and was instead removed. After filtering the 9166 spatial groups for isolation condition determination, 1284 spatial groups remained. Fig. 5 shows the example results of several airports after scene classification and post-processing.

### B. Airport Detection and Geographic Analysis Results

After the runway detection model was performed on the 1284 spatial groups, the results with scores greater than the threshold (0.59 recommended) were saved, and 354 detection boxes were ultimately obtained as low confidence airports. Based on the above spatial distribution constraints, main direction constraints, side length constraints, and spatial fusion, a total of 52 airport points from 354 runways were extracted. Subsequently, 23 out of 52 low-confidence airports were detected with aircraft, which were updated as high-confidence airports.

Fig. 6 shows the recalls of known airports; a total of 27 were recalled, and one was lost.

### C. Systematic Validation

The above calculation framework was used for unknown airport target detection in the entire 21 9040.5 km$^2$ study area (Jiangsu, Shanghai, and Zhejiang) by combining deep learning and comprehensive geographic analysis; as a result, 52 airport points with different confidence candidate areas were obtained (see Fig. 7). Through systematic verification, eight airports were "newly discovered," 35 of the 52 blocks were correctly identified, 27 were recalled and 1 was lost from known airports, while 36 airports were obtained manually in the study area. Among the 35 correctly identified results, there were 23 high-confidence airports, among which 3 were newly discovered airports, and there were 12 low-confidence airports, of which 5 were newly discovered airports. The known airport recall rate of these models and framework was 96.4%, and the airport integrity rate (integrity rate is calculated as the ratio of the number of airports under this framework to the number of airports searched visually) was 97.2%; the speed was approximately 20 times faster than that of a traditional visual search. However, an airport discovered near a known airport was judged as belonging to the same candidate area if the distance between the two was less than the threshold. Finally, a relatively complete and correct airport point database for the study area was obtained. The specific situation is summarized in Fig. 7, and the newly discovered airport images are tagged.

TABLE III
RUNNING EFFICIENCY STATISTICS

| Methods | Type | Accuracy | Time (s) |
|---|---|---|---|
| Framework of this paper | Candidate area extraction | 2.0% | 39890 |
| | Airport confidence evaluation (runway and aircraft included) | 10.2% | 1203 |
| | Geographic analysis | 67.3% | 419(Internal constraints 403s, external constraints 16s) |
| | Systematic verification | 100% | 250 |
| | **Total** | **-** | **41762** |
| Direct runway detection throughout the study area | Runway detection | 1.2% | 40057 |
| | Systematic verification | 100% | 14992 |
| | **Total** | **-** | **55049** |
| Traditional visual search | Systematic verification | 100% | **818535** |

TABLE IV
PERFORMANCE OF THE MODELS

| Methods | Test-samples | Accuracy | Recall |
|---|---|---|---|
| Scene classification | 22674 | 93.6% | 98.7% |
| Runway detection [47] | 3840 | 92.8% | 85.1% |
| Aircraft detection [3] | 760 | 94.2% | - |

### D. Running Efficiency Statistics

In Table III, we have calculated the running efficiency of the framework in this article and compared the results of direct runway detection in the study area and those of traditional visual searches. The results show that the combined methods utilized in this framework are superior to direct runway detection and traditional visual search. Although traditional visual searches are guaranteed to find all airports, they can be extremely time-consuming.

## IV. DISCUSSION

### A. Performance of the Models in This Framework

For the scene classification model in the candidate area extraction, the network structure of the ImageNet pretrained model was frozen, and the newly added layers were trained in the early 20 epochs of training. At this stage, the learning rate was set to 0.001. In the later stage of training, the learning rate was adjusted to 0.00005 while the frozen network was thawed and the training continued. Finally, we trained 36 epochs to obtain the scene classification model of the study area; its training loss, training accuracy, verification loss, and verification accuracy were 0.0301, 0.9920, 0.0351, and 0.9888, respectively. The dropout regularization parameter was set to 0.5 for the entire training process.

A total of 22 674 tiles were selected as testing samples. Of those, 15 513 negative samples were within the study area and 93 positive samples were around the study area, which were increased to 7161 according to the augmentation methods mentioned in the framework. After sample testing, 15 438 negative samples are correctly classified and 5775 positive samples are correctly classified; therefore, the overall accuracy was 93.6% and the recall rate of the runway tiles was 98.7%. The performance of the runway detection model and aircraft detection model are shown in Table IV according to [3] and [47], respectively.

### B. Airport Loss and Errors

Twenty-eight airports with evident runways in the study area were obtained from the public database of OA; however, only 27 known airports were ultimately recalled, and one was lost in Shanghai. In the "missing" airport, the position of the runway box was easily recognized while performing runway detection. However, the "secondary" roads near the airport (considered "secondary" based on the accuracy of the data) caused the road network and the actual roads to have a large difference in geographic location when the road network in the OSM data was used for spatial distribution constraints. Thus, the runway crossed the road, and the airport was mistakenly lost. We also found that general misidentification mainly included water canals, rivers, roads, etc. The Jiangsu-Zhejiang region has been known as the "land of fish and rice" since ancient times, and its irrigation canals, rivers, roads, and other economic factors have been relatively developed. However, this kind of data is excessively detailed. The width of the general irrigation channel is only approximately 1 m; thus, it cannot be easily reflected in the OSM data. Moreover, some river elements are not complete in the OSM data, and thus, the results cannot be constrained for the missing data.

In summary, several detection errors were caused by the specific development of the study area and the quality of data. If the refined data of the study area can be obtained, the detection accuracy will improve.

### C. Geoscience Restraint Ability

This section focuses on the analysis of the constraint ability of different geographic data or geographic thresholds on the

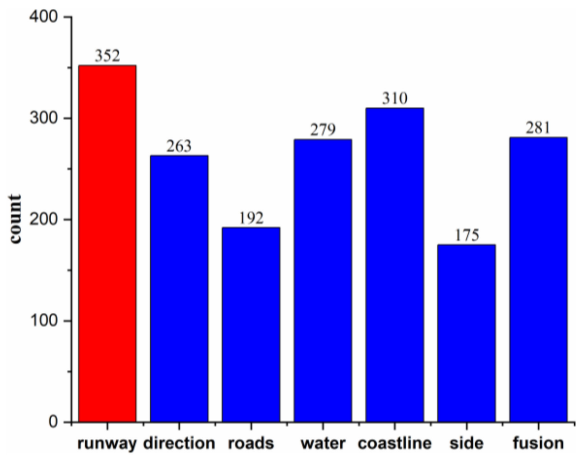


Fig. 8. Constraint abilities of different methods.

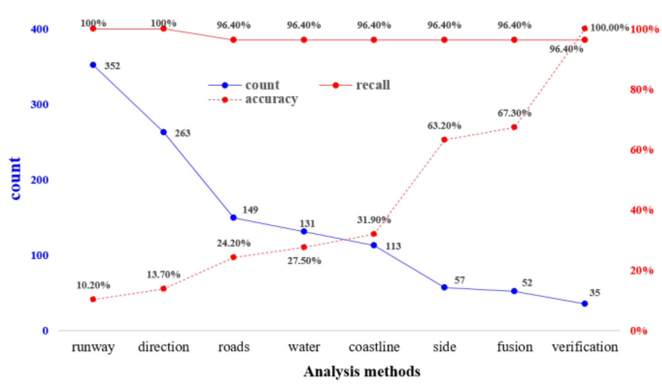


Fig. 9. Result changes under different steps.

detection results. The sequences of different steps did not affect the results, ultimately, the restraint ability of the different methods is what is important. As shown in Fig. 8, the constraints are expressed under the results of different geographic analysis calculation methods: after only the main direction constraint was applied, the remaining runway results numbered 263; the resulting numbers solely constrained by the road space distribution, the water system's spatial distribution, the coastline's spatial distribution, the side length, and spatial fusion were 192, 279, 310, 175, and 281, respectively.

A progressive method was taken to constrain the runway results and different constraint methods overlapped. Based on the steps in this study, the changes in the number of remaining runways, the recall rate of known airports, and the accuracy of extracted results are shown in Fig. 9. The final systematic verification is to ensure the absolute correctness of the extraction results.

## D. Geographical Differences With Scene Classification Model

Owing to the influences of various economic, cultural, geographical, and other comprehensive factors, different regions exhibit unique surface differences, and their airport construction and development levels are also highly variant, as shown in

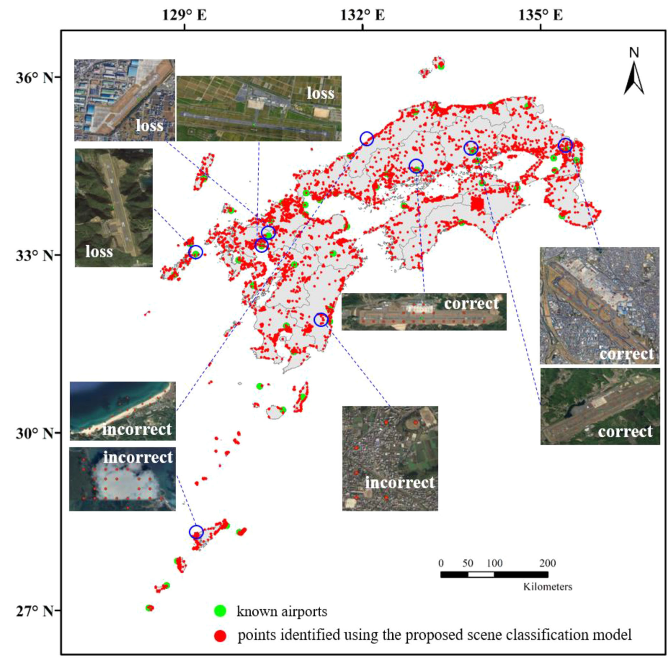


Fig. 10. Results of the proposed scene classification model in 19 counties of Japan.

Fig. 8. To study the prediction ability of the scene classification model in other regions, we conducted scene classification experiments on 19 counties of Japan (as shown in Fig. 10). In the OA database, there are 52 airports with evident runways in the studied regions of Japan.

Fig. 10 demonstrates that some airports were correctly classified, which meant that the scene classification model first trained within the study area of this research had a certain positive effect on detection accuracy in other areas. However, some airport scenes were not correctly identified, which caused several potential airports to be lost, while others were incorrectly identified. We posit that the accuracy will positively correlate with surface differences owing to different factors such as geography, economy, and culture. In using the proposed framework, the applicability of the model between different regions must comprehensively consider the differences between regions, and the quantitative expression of these differences requires further study.

# V. Conclusion

We proposed a framework for unknown airport detection in broad area scenes. The framework combined with deep learning and geographic analysis calculations formed a relatively complete and current database of airports in the research area. The proposed framework improved the discovery rate of airports with varying confidence in the target area, which, in turn, expanded the known airport database and broadened the potential applications of deep learning in the field of remote sensing. In future research, we will use our methodology to perform airport detections globally.

The accuracy of the framework is easily constrained by geographic data. Relatively high-quality data and models are the keys to achieving a high-precision framework. Concurrently, model migration in different regions is affected by the surface coverage, and we believe that the main reasons for this phenomenon are the influences of geography, economy, and cultural factors. Determining how to divide the geographic space, how to build the most universal model possible, and studying the generalization ability of data and models are all topics in need of further study.

In general, the proposed framework can improve airport detection rates in a broad area and the quality and quantity of existing data. In addition, it provides technical ideas for searching for other large targets in broad areas and has a certain reference value.

## References

[1] S. Yin, H. Li, and L. Teng, "Airport detection based on improved faster RCNN in large scale remote sensing images," *Sensing Imag.*, vol. 21, no. 1, Oct. 2020, Art. no. 49, doi: 10.1007/s11220-020-00314-2.

[2] F. Chen, R. Ren, T. Van de Voorde, W. Xu, G. Zhou, and Y. Zhou, "Fast automatic airport detection in remote sensing images using convolutional neural networks," *Remote Sens.*, vol. 10, no. 3, Mar. 2018, Art. no. 443, doi: 10.3390/rs10030443.

[3] F. Zeng *et al.*, "A hierarchical airport detection method using spatial analysis and deep learning," *Remote Sens.*, vol. 11, no. 19, Jan. 2019, Art. no. 2204, doi: 10.3390/rs11192204.

[4] X. Yao, J. Han, L. Guo, S. Bu, and Z. Liu, "A coarse-to-fine model for airport detection from remote sensing images using target-oriented visual saliency and CRF," *Neurocomputing*, vol. 164, pp. 162–172, Sep. 2015, doi: 10.1016/j.neucom.2015.02.073.

[5] T. Gefu, X. Zhifeng, L. Qing, and L. Hua, "A novel airport detection method via line segment classification and texture classification," *IEEE Geosci. Remote Sens. Lett.,* vol. 12, no. 12, pp. 2408–2412, Dec. 2015.

[6] U. Budak, U. Halici, A. Sengur, M. Karabatak, and Y. Xiao, "Efficient airport detection using line segment detector and fisher vector representation," *IEEE Geosci. Remote Sens. Lett.,* vol. 13, no. 8, pp. 1079–1083, Aug. 2016.

[7] Z. Xiao, Y. Gong, Y. Long, D. Li, X. Wang, and H. Liu, "Airport detection based on a multiscale fusion feature for optical remote sensing images," *IEEE Geosci. Remote Sens. Lett.,* vol. 14, no. 9, pp. 1469–1473, Sep. 2017.

[8] J. Wang, G. Zhang, K. Zhang, Y. Zhao, Q. Wang, and X. Li, "Detection of small aerial object using random projection feature with region clustering," *IEEE Trans. Cybern.*, to be published, doi: 10.1109/TCYB.2020.3018120.

[9] Y. Yuan, Z. Xiong, and Q. Wang, "VSSA-NET: Vertical spatial sequence attention network for traffic sign detection," *IEEE Trans. Image Process.*, vol. 28, no. 7, pp. 3423–3434, Jul. 2019.

[10] J. Yuan, H. H. L. Yang, O. A. Omitaomu, and B. L. Bhaduri, "Large-scale solar panel mapping from aerial images using deep convolutional networks," in *Proc. IEEE Int. Conf. Big Data*, Dec. 2016, pp. 2703–2708.

[11] R. A. Marcum, C. H. Davis, G. J. Scott, and T. W. Nivin, "Rapid broad area search and detection of Chinese surface-to-air missile sites using deep convolutional neural networks," *J. Appl. Remote Sens.*, vol. 11, no. 4, 2017, Art. no. 042614, doi: 10.1117/1.JRS.11.042614.

[12] J. Yu, Z. Wang, A. Majumdar, and R. Rajagopal, "DeepSolar: A machine learning framework to efficiently construct a solar deployment database in the united states," *Joule*, vol. 2, no. 12, pp. 2605–2617, Dec. 2018, doi: 10.1016/j.joule.2018.11.021.

[13] G. J. Scott, J. A., Hurt R. A. Marcum, D. T. Anderson, and C. H. Davis, "Aggregating deep convolutional neural network scans of broad-area high-resolution remote sensing imagery," in *Proc. IEEE Int. Geosci. Remote Sens. Symp.*, Jul. 2018, pp. 665–668.

[14] P. Gong *et al.*, "Stable classification with limited sample: Transferring a 30-m resolution sample set collected in 2015 to mapping 10-m resolution global land cover in 2017," *Sci. Bull.*, vol. 64, no. 6, pp. 370–373, Mar. 2019, doi: 10.1016/j.scib.2019.03.002.

[15] S. Ren, K. He, R. Girshick, and J. Sun, "Faster R-CNN: Towards real-time object detection with region proposal networks," *IEEE Trans. Pattern Anal. Mach. Intell.,* vol. 39, no. 6, pp. 1137–1149, Jun. 2017.

[16] K. He, X. Zhang, S. Ren, and J. Sun, "Deep residual learning for image recognition," in *Proc. IEEE Conf. Comput. Vis. Pattern Recognit.*, Jun. 2016, pp. 770–778.

[17] C. Szegedy *et al.*, "Going deeper with convolutions," in *Proc. IEEE Conf. Comput. Vis. Pattern Recognit.*, Jun. 2015, pp. 1–9.

[18] S. Bo and Y. Jing, "Region-based airplane detection in remotely sensed imagery," in *Proc. 3rd Int. Congr. Image Signal* , Oct. 2010, pp. 1923–1926, doi: 10.1109/CISP.2010.5647478.

[19] Q. Luo and Z. Shi, "Airplane detection in remote sensing images based on object proposal," in *Proc. IEEE Int. Geosci. Remote Sens. Symp.*, Jul. 2016, pp. 1388–1391.

[20] Z. Chen, T. Zhang, and C. Ouyang, "End-to-end airplane detection using transfer learning in remote sensing images," *Remote Sens.*, vol. 10, no. 1, Jan. 2018, Art. no. 139, doi: 10.3390/rs10010139.

[21] Y. Xu, M. Zhu, P. Xin, S. Li, M. Qi, and S. Ma, "Rapid airplane detection in remote sensing images based on multilayer feature fusion in fully convolutional neural networks," *Sensors*, vol. 18, no. 7, Jul. 2018, Art. no. 2335, doi: 10.3390/s18072335.

[22] M. Zhu, Y. Xu, S. Ma, S. Li, H. Ma, and Y. Han, "Effective airplane detection in remote sensing images based on multilayer feature fusion and improved nonmaximal suppression algorithm," *Remote Sens.*, vol. 11, no. 9, May 2019, Art. no. 1062, doi: https://doi.org/10.3390/rs11091062.

[23] L. Zhang and Y. Zhang, "Airport detection and aircraft recognition based on two-layer saliency model in high spatial resolution remote-sensing images," *IEEE J. Sel. Topics Appl. Earth Observ. Remote Sens.,* vol. 10, no. 4, pp. 1511–1524, Apr. 2017.

[24] W. Zhang, W. Lv, Y. Zhang, J. Tian, and J. Ma, "Unsupervised-learning airplane detection in remote sensing images," in *Proc. MIPPR, Remote Sens. Image Process., Geographic Inf. Syst., Other Appl.*, 2015, vol. 9815, Art. no. 981503, doi: 10.1117/12.2205827.

[25] X. Li and S. Wang, "Object detection using convolutional neural networks in a coarse-to-fine manner," *IEEE Geosci. Remote Sens. Lett.,* vol. 14, no. 11, pp. 2037–2041, Nov. 2017.

[26] W. Guo, W. Yang, H. Zhang, and G. Hua, "Geospatial object detection in high resolution satellite images based on multi-scale convolutional neural network," *Remote Sens.,* vol. 10, no. 1, Jan. 2018, Art. no. 131, doi: 10.3390/rs10010131.

[27] N. Liu, Z. Cui, Z. Cao, Y. Pi, and S. Dang, "Airport detection in large-scale SAR images via line segment grouping and saliency analysis," *IEEE Geosci. Remote Sens. Lett.,* vol. 15, no. 3, pp. 434–438, Mar. 2018.

[28] D. Zhao, J. Li, Z. Shi, Z. Jiang, and C. J. I. A. Meng, "Subjective saliency model driven by multi-cues stimulus for airport detection," *IEEE Access*, vol. 7, no. 99, pp. 32118–32127, Feb. 2019.

[29] T. Zhu, Y. Li, Q. Ye, H. Huo, and T. Fang, "Integrating saliency and resnet for airport detection in large-size remote sensing images," in *Proc. 2nd Int. Conf. Image, Vis. Comput.*, Jun. 2017, pp. 20–25, doi: 10.1109/ICIVC.2017.7984451.

[30] Z. Dan, W. Bin, and Z. Liming, "Airport target detection in remote sensing images: A new method based on two-way saliency," *IEEE Geosci. Remote Sens. Lett.,* vol. 12, no. 5, pp. 1096–1100, May 2015.

[31] Q. Zhang, L. Zhang, W. Shi, Y. J. I. G. Liu, and R. S. Letters, "Airport extraction via complementary saliency analysis and saliency-oriented active contour model," *IEEE Geosci. Remote Sens. Lett.*, vol. 15, no. 7, pp. 1085–1089, May 2018.

[32] X. R. Sun, W. B. Sun, and L. I. De-Jun, "Detection and analysis for synthetic aperture radar image of airport," *DEStech Trans. Eng. Technol. Res.*, no. icicr, 2019, doi: 10.12783/dtetr/icicr2019/30563.

[33] P. Zhang, X. Niu, Y. Dou, and F. Xia, "Airport detection on optical satellite images using deep convolutional neural networks," *IEEE Geosci. Remote Sens. Lett.,* vol. 14, no. 8, pp. 1183–1187, Aug. 2017.

[34] Y. Wang, C. Wang, H. Zhang, Y. Dong, and S. J. R. S. Wei, "Automatic ship detection based on RetinaNet using multi-resolution Gaofen-3 imagery," *Remote Sens.*, vol. 11, no. 5, 2019, Art. no. 531, doi: 10.3390/rs11050531.

[35] S. Li, Y. Xu, M. Zhu, S. Ma, H. J. I. G. Tang, and R. S. Letters, "Remote sensing airport detection based on end-to-end deep transferable convolutional neural networks," *IEEE Geosci. Remote Sens. Lett.,* vol. 16, no. 10, pp. 1640–1644, Oct. 2019.

[36] Ö. Aytekin, U. Zongur, U. J. I. G. Halici, and R. S. Letters, "Texture-based airport runway detection," *IEEE Geosci. Remote Sens. Lett.*, vol. 10, no. 3, pp. 471–475, Aug. 2013.

[37] D. Zhao, Y. Ma, Z. Jiang, Z. Shi, and R. Sensing, "Multiresolution airport detection via hierarchical reinforcement learning saliency model," *IEEE J. Sel. Topics Appl. Earth Observ. Remote Sens.*, vol. 10, no. 6, pp. 2855–2866, Jun. 2017.

[38] Q. Wang, W. Huang, Z. Xiong, and X. Li, "Looking closer at the scene: Multiscale representation learning for remote sensing image scene classification," *IEEE Trans. Neural Netw. Learn. Syst.*, to be published, doi: 10.1109/TNNLS.2020.3042276.

[39] J. Redmon, S. Divvala, R. Girshick, and A. Farhadi, "You only look once: Unified, real-time object detection," in *Proc. IEEE Conf. Comput. Vis. Pattern Recognit.*, Jun. 2016, pp. 779–788.

[40] J. Redmon and A. Farhadi, "YOLO9000: Better, faster, stronger," in *Proc. IEEE Conf. Comput. Vis. Pattern Recognit.*, Jul. 2017, pp. 6517–6525. Accessed: May, 7, 2020. [Online]. Available: http://arxiv.org/abs/1612.08242

[41] J. Redmon and A. Farhadi, "YOLOv3: An incremental improvement," Apr. 2018. Accessed: May 7, 2020. [Online]. Available: https://arxiv.org/abs/1804.02767v1

[42] W. Liu, D. Anguelov, D. Erhan, C. Szegedy, and A. C. Berg, "SSD: Single shot multibox detector," in *Proc. Eur. Conf. Comput. Vis.*, Sep. 2018, pp. 21–37, doi: 10.1007/978-3-319-46448-0_2.

[43] R. J. C. E. and Girshick, "Fast R-CNN," in *Proc. IEEE Int. Conf. Comput. Vis.*, Dec. 2015, pp. 1440–1448.

[44] S. Ren, K. He, R. Girshick, J. Sun, and M. Intelligence, "Faster R-CNN: Towards real-time object detection with region proposal networks," in *Proc. Advances in Neural Inf. Proc. Syst.*, Dec. 2015, pp. 91–99, doi: 10.1109/TPAMI.2016.2577031.

[45] X. Sun, S. Wandelt, M. J. N. Hansen, and S. Economics, "Airport road access at planet scale using population grid and openstreetmap," *Netw. Spatial Econ.*, vol. 20, no. 1, pp. 273–299, 2020, doi: 10.1007/s11067-019-09480-7.

[46] M. Haklay and P. J. I. P. C. Weber, "OpenStreetMap: User-generated street maps," *IEEE Pervasive Comput.*, vol. 7, no. 4, pp. 12–18, Oct.–Dec. 2008.

[47] C. Ji, L. Cheng, N. Li, F. Zeng, M. Li, and R. Sensing, "Validation of global airport spatial locations from open databases using deep learning for runway detection," *IEEE J. Sel. Topics Appl. Earth Observ. Remote Sens.*, vol. 14, pp. 1120–1131, 2021, doi: 10.1109/JSTARS.2020.3034609.

[48] R. G. V. Gioi, J. Jakubowicz, J. M. Morel, and G. J. I. P. O. L. Randall, "LSD: A line segment detector," *Image Process. Line*, vol. 2, no. 4, pp. 35–55, 2012, doi: 10.5201/ipol.2012.gjmr-lsd.


**Ning Li** received the B.Sc. degree in geographic information science from Chang'an University, Xi'an, China, in 2018. He is currently working toward the Ph.D. degree in geography from Nanjing University, Nanjing, China.

His research interests include deep learning and remote sensing applications.

**Liang Cheng** received the Ph.D. degree in photogrammetry and remote sensing from Wuhan University, Wuhan, China, in 2008.

He is currently a Professor with the Jiangsu Provincial Key Laboratory of Geographic Information Science and Technology, Nanjing University, Nanjing, China. His current research interests include integration of multisource spatial data and remote sensing image processing.

**Lingyong Huang** received the Ph.D. degree in survey and mapping from Zhengzhou University of Information Engineering, Zhengzhou, China, in 2015.

His research interest focuses on remote sensing applications.

**Chen Ji** received the B.Eng. degree in surveying and mapping from Nanjing Normal University, Nanjing, China, in 2013, and the M.E. degree in geographic information system from Beijing Normal University, Beijing, China, in 2016. He is currently working toward the Ph.D. degree in geography from Nanjing University, Nanjing, China.

His research interests include deep learning, GIS, and remote sensing applications.

**Min Jing** received the B.Sc. degree in geographic information science from YunNan University, Yunnan, China, in 2016, and the M.E. degree in surveying and mapping from Nanjing Normal University, Nanjing, China, in 2019. She is currently working toward the Ph.D. degree in geography from Nanjing University, Nanjing, China.

Her research interests include GIS and remote sensing applications.

**Zhixin Duan** received the B.Eng. degree in remote sensing science and technology from Chang'an University, Xi'an, China, in 2016, and the MA.Sc. degree in surveying and mapping science and technology from China University of Mining and Technology, Xuzhou, China, in 2019. He is currently working toward the Ph.D. degree in geography from Nanjing University, Nanjing, China.

**Jingjing Li** received the B.Sc. degree in electronic information science and technology from Shandong University of Technology, Zibo, China, in 2010.

Her research interest focuses on remote sensing applications.

**Manchun Li** received the Ph.D. degree in cartography from Nanjing University, Nanjing, China, in 1992.

He is currently a Professor with the Jiangsu Provincial Key Laboratory of Geographic Information Science and Technology, Nanjing University. His research interests include GIS and remote sensing applications.